

Development and characterization of a new adsorbent based on Jerivá coconut (*Syagrus romanzoffiana*) applied for removing toxic metals from water

Joceane Pigatto^a, Danieli Brandler^b, Gabriel Tochetto^b, Deisy M. Memlak^a, Gean D.L.P. Vargas^b, Alcione Aparecida de Almeida Alves^b, Liziane Schittler Moroni^a, Anieli Pinto Kempka^a, Cleuzir da Luz^a, Adriana Dervanoski^{b,*}

^aFood Engineering Department, Santa Catarina State University, BR 282, Km 573, 89870-000 Pinhalzinho, Santa Catarina, Brazil, emails: jocepigatto@gmail.com (J. Pigatto), deisymemlak@gmail.com (D.M. Memlak), liziane.schittler@udesc.br (L.S. Moroni), anieli.kempka@udesc.br (A.P. Kempka), cleuzir.luz@udesc.br (C. da Luz)

^bEnvironmental Engineering and Sanitary, Federal University of Fronteira Sul, ERS 135, Km 72, 99700-970 Erechim, Rio Grande do Sul, Brazil, Tel. +55 (54) 3321-7336; Fax: +55 (54) 3321-7336; emails: adriana.dervanoski@uffs.edu.br (A. Dervanoski), danielibrandler@gmail.com (D. Brandler), tochetto gabriel@gmail.com (G. Tochetto), geandelise@uffs.edu.br (G.D.L.P. Vargas), alcione.almeida@uffs.edu.br (A.A.A. Alves)

Received 28 March 2019; Accepted 25 March 2020

ABSTRACT

This study developed a new adsorbent based on Jerivá coconut (*Syagrus romanzoffiana*), palm native from the Brazilian Atlantic Forest, for application in the monocomponent removal of toxic metallic ions present in a synthetic water matrix, such as Ni²⁺, Cd²⁺, Cu²⁺, and Zn²⁺. The characterization and experimental data showed that the raw material of natural source is a potential adsorbent. The adsorption trials showed that the developed adsorbent has affinity for the metallic ions and they preferably followed the Langmuir model. The adsorption was influenced by temperature. Greater adsorption capacity occurred for Ni²⁺, followed by Cu²⁺, Cd²⁺, and Zn²⁺. The thermodynamic parameters, such as ΔH° , ΔS° , and ΔG° indicated endothermic, spontaneous, and favorable adsorption for ions Ni²⁺, Cd²⁺, and Zn²⁺, and non-spontaneous for Cu²⁺. The results demonstrated that the adsorbent has potential for use in the treatment process of supply water contaminated with toxic metals.

Keywords: Adsorption; Jerivá coconut; New adsorbent; Characterization; Heavy metal

1. Introduction

The accumulation of metallic ions in human bodies occurs mainly by ingesting food [1] or by the direct ingestion of contaminated water. In Brazil, consolidation of decree n° 5/2017, of the Ministry of Health, disposes on the control and surveillance procedures of the quality of water for human consumption and its potability standards [2].

Adsorption is a prominent process among the economically feasible and effective technologies for removing trace amounts of metallic ions in water. According to

Tounsadi et al. [3], adsorption using activated carbon is one of the simplest and most effective methods, which can be produced from various sources. However, the depletion of this resource encourages research using renewable materials and natural sources.

Studies on low-cost adsorbents applied to the removal of toxic metals can be found in literature, such as the work of Sousa et al. [4], who evaluated the use of the husk of green coconut, a biodegradable agroindustrial residue, to remove Pb²⁺, Ni²⁺, Cd²⁺, Zn²⁺, and Cu²⁺ ions, shown to be a feasible alternative to treat potable water.

* Corresponding author.

Activated carbons are artificial materials characterized by the high surface area and a great volume of pores, in addition to presenting extensive surface chemistry, which is responsible for the significant adsorptive properties of the materials [5–7]. It is possible to develop activated carbons for distinct applications when the contaminant to be removed is known. Since the first studies conducted on the removal of metallic ions, activated carbon was doubtless the most popular and widely used as an adsorbent to treat water all over the world [7–9]. Despite its vast use, these adsorbents are still an expensive material, with cost proportional to its quality. Therefore, there is increasing interest in finding alternative adsorbents, seeking cost reduction without decreasing the efficiency of the adsorption process [10].

In recent decades, the industry of activated carbon has used materials derived from natural sources and a few agricultural [11] and industrial [12] residues, with the objective of appreciating such residues or byproducts [6].

Natural materials are presented as potential low-cost adsorbent sources, given their availability in large quantities, often residues of agricultural operations [7,13–15], such as husks, sawdust, and wheat bran, offering low economic value and presenting problematic disposal [1,16]. Many authors report the adsorption of heavy metals using a variety of low-cost activated carbons, such as sugarcane bagasse [17], peanut husk [1], almond husk, rice peel ash [16], coconut fiber and husk [18,19], cellulose adsorbents,¹⁵ among others. According to Nabais et al. [6], the use of such materials corresponds to the production of more than 300 thousand tons of activated carbon per year, being wood and coconut husk the most relevant materials.

Among the possible adsorbents from renewable natural sources, Jerivá (*Syagrus romanzoffiana*) is a palm of the Arecaceae family, native to the Atlantic Forest and associated ecosystems in Brazil, such as restinga, dense ombrophylouse forests, semi-deciduous seasonal forests, deciduous seasonal forests, or other forestry formations, such as ciliary forests, swamp forests, and cerrado, growing in locations of tropical climate and capable of tolerating low temperatures [20]. It is a single stalk palm, reaching up to 20 m of height [21], and 30 m in the middle of the forest, with a stalk of 25–45 cm of diameter. The inflorescence is interfoliar, emerging from within a woody and fissured spadix of up to 26 cm of length, held by the peduncle. When the spadix opens, thousands of flowers emerge, with fruits denominated Jerivá coconut. The external portion of the fruit is fleshy, ovulated, and of yellow or orange coloration [20]. Internally, it presents a small chestnut similar to cocoda-baía [22]. It has abundant production of fruits in a wide period of the year.

This adsorbent development study using the Jerivá coconut is unprecedented. Understanding the production mechanisms of an efficient adsorbent, such as the production of activated carbon, such as functional surface groups, surface area, solid density, and micrographs of the physical structure, is necessary to produce activated carbon from this fruit, in addition to evaluating the application potential of adsorbent carbon. Due to this, this study aimed at developing and characterizing a new adsorbent using the thermally treated Jerivá coconut, which is economically feasible, accessible, and it presents the potential application for removing

monocomponent toxic metals present in water supply and effluent.

2. Material and methods

2.1. Materials

The adsorbent used was obtained from the fruit, in the unripe phase, of *Syagrus romanzoffiana*. The fruit was collected in the northern region of Rio Grande do Sul, Brazil. The solutions of metallic ions were prepared with deionized water based on their respective salts: $\text{CdSO}_4 \cdot 8/3\text{H}_2\text{O}$, $\text{CuSO}_4 \cdot 5\text{H}_2\text{O}$, $\text{ZnSO}_4 \cdot 7\text{H}_2\text{O}$, $\text{NiSO}_4 \cdot 6\text{H}_2\text{O}$ (Vetec), with pH of approximately 5.5 (pH was chosen based on the solubility curve, concentration vs. pH for the metals studied). To read the concentration of the remaining metals in the solution, after adsorption, an atomic absorption spectrometer of continuous high-resolution source was used, coupled to automatic sampler (AnalytikJena – ContrAA 700), using a validated methodology [23].

2.2. Methods

2.2.1. Adsorbent development

After harvest, the Jerivá coconut (*Syagrus romanzoffiana*) was taken for drying in an oven. Subsequently, the material was ground, carbonized, and pyrolyzed at 500°C in furnace (Lavoisier, Model 400 D) for 2 h and 30 min, time determined by preliminary tests. After being carbonized and pyrolyzed, the adsorbent was sieved in 60 mesh, conditioned in polyethylene flasks and stored in desiccator.

2.2.2. Adsorbent characterization

The adsorbent was characterized by the following trials: particle size, moisture tests, volatile material, ashes, and fixed carbon. Experiments were conducted to determine the surface functional groups using the Boehm titrimetric method, Fourier transform infrared spectroscopy (FTIR), and point of zero charge (PZC) of the activated carbon. Helium gas pycnometry was used to determine the real density and porosity of the solid. The Brunauer–Emmett–Teller (BET) and Barrett–Joyner–Halenda (BJH) tests were conducted to determine the surface area, pore volume, pore size distribution, and particle irregularity of the studied material. Scanning electron microscopy (SEM) was used to obtain the micrographs of the physical structure of the sample.

2.2.2.1. Particle size

The determination of particle size was done by conducting granulometric analysis, placing 100 or 200 g of activated carbon in sieves with standard mesh, which are mechanically agitated for at least 15 min (sieve agitator of the Minor Endecotts brand). The activated carbon retained in each sieve was separated and stored.

2.2.2.2. Moisture, volatile material, and fixed carbon contents

The moisture of the carbon was determined by heating the known mass at the temperature of 105°C in oven (Biopar,

Modelo B22ST), until stabilizing the weight. Moisture was obtained with the difference between the initial and final weights of the sample. After this stage, the remaining sample was placed in a furnace (Lavoisier, Model 400 D) at 950°C for approximately 5–7 min, cooled in desiccator and weighed, thus obtaining the volatile material content. To determine the ash content, the residual material of the previous analysis was placed in furnace, initially at room temperature, increasing until reaching 800°C, remaining until all the material was burnt. Subsequently, the residue was removed from the furnace, cooled in desiccator, and weighed. The contents of ash and fixed carbon were obtained by the difference between the initial and final weights [24].

2.2.2.3. Determination of the functional surface groups

The determination of the surface functional groups was done using the Boehm titrimetric method [25,26], in which 2 g of the activated carbon sample was placed in contact with 50 mL of 0.1 N of the following solutions: NaOH, Na₂CO₃, NaHCO₃, and HCl. The flasks were sealed and agitated in Shaker (EQUILAM, model IB 9082A) for 24 h. After this period, the samples were filtered, obtaining aliquots of 10 mL. Respectively 15, 15, and 20 mL of the standard HCl (0.1 N) solution were added to the aliquot of NaOH, Na₂CO₃, and NaHCO₃, along with the phenolphthalein indicator, performing a back titration with NaOH (0.1 N) solution. Phenolphthalein was added to an aliquot of HCl with further titration with standard NaOH (0.1 N) solution. The white tests (with no activated carbon) were performed according to the same methodology. The number of acid groups was determined considering that NaOH neutralizes the carboxyl, lactones, and phenolic groups; Na₂CO₃ neutralizes carboxylic and lactone groups; and NaHCO₃ neutralizes only carboxylic groups. The carboxylic groups were determined by titrating the aliquot of Na₂CO₃. The lactones groups were determined using the difference between the results of the Na₂CO₃ and NaHCO₃ titration. The phenolic groups were determined by the difference between the results found in the titration of NaOH and NaHCO₃. The number of basic sites was calculated considering the amount of HCl that reacted with carbon. All solutions were standardized before the titrimetric trials.

Eq. (1) was used to calculate the acids group:

$$mEq_{g(GA)} = \frac{V_t \times N_a \times (V_{am} - V_b)}{V_{al}} \quad (1)$$

In which, V_b and V_{am} are the volumes of the NaOH standard solution expended in the titration of the white and aliquots, respectively (mL); V_t is the volume of HCl solution used in adsorption (mL); V_{al} is the volume of the filtrated aliquot used for titration (mL), and N_a is the concentration of HCl solution.

Eq. (2) was used to calculate the basic groups:

$$mEq_{g(GB)} = \frac{V_t \times N_b \times (V_b - V_{am})}{V_{al}} \quad (2)$$

In which N_b is the concentration of the NaOH solution.

2.2.2.4. Fourier transform infrared spectroscopy

Attenuated total reflection (ATR) FTIR, was used to determine the surface functional groups of the samples. ATR is used since the analysis consists of a solid with adsorbent capacity. The samples were analyzed at room temperature, with a scanning range of 200–4,000 cm⁻¹. The samples of the developed adsorbent material were washed in excess water to ensure the removal of possible contaminants. Subsequently, the samples were dried at 85°C for approximately 12 h to minimize the effect of moisture on the spectrum. The thermal drying of the carbon presented low-graduation not to alter the structure of the material. Posteriorly, samples were measured using an infrared spectrometer (SHIMADZU – Model IR Prestige 21, Greece).

2.2.2.5. Point of zero charge

The PZC indicates the pH value in which the solid presents charge electrically null on its surface, denoted by pH_{PZC}. The surface of the adsorbent will be neutral when the pH value is equal to the pH_{PZC} value. For pH values higher than that of the surface (pH_{PZC}) of the adsorbent, the adsorbent becomes negatively charged, and for pH values inferior to pH_{PZC}, there will be positive charges on the surface of the adsorbent [27,28]. The pH_{PZC} was obtained by means of 12 solutions of 50 mL of deionized water added with adequate amounts of HCl and NaOH in pH values ranging from 1 to 12. Subsequently, 0.1 ± 0.0001 g of the adsorbent was added under agitation in the shaker at 140 rpm, for 24 h, at room temperature [27,28]. After 24 h, the pH was measured with pH meter of the Tecnopon brand.

2.2.2.6. Helium gas pycnometry

A helium gas pycnometry trial was conducted to determine the real density of the studied adsorbent. This trial was performed in Ultrapyc Pycnometer 1200e (Quantachrome instruments) from samples dried in an oven for 12 h at 100°C.

2.2.2.7. BET adsorption

BET adsorption isotherm was used to calculate the surface area of the microporous adsorbents. Created in 1938, by Brunauer et al. [29] the method is based on the determination of the volume of nitrogen adsorbed at various pressures, at the temperature of liquid nitrogen, employed in the equation deduced by them, allowing the determination of the volume of nitrogen necessary to form a monomolecular layer over the adsorbed material. To do so, the volume of the monolayer is obtained by the volume of gas adsorbed at a certain pressure. To conduct the adsorption trial, approximately 100 mg of the sample of activated carbon were weighed and placed in a quartz crystal cell, in which the samples were prepared to remove the residual moisture and remaining volatiles present. To do that, the samples underwent a degassing process in a gas station of the equipment, in which they remained for 20 h, at 200°C, and under 0.1 mm Hg vacuum. After this treatment, the sample was conditioned in an analysis station, where it remained immersed in liquid nitrogen during all the trials to maintain thermal stability.

2.2.2.8. Barrett–Joyner–Halenda

Barret et al. [30] developed a mathematical method denominated BJH, which is used until now to calculate the distribution of the pore sizes. The method uses the Kelvin equation and it assumes the progressive emptying of the pores filled with liquid, with the decrease in pressure. It can be applied for both adsorption and desorption, since the decrease in pressure begins where the pores are considered completely full, normally for P/P_0 equal to 0.95, or at a pressure of 95% of saturation.

2.2.2.9. Scanning electron microscopy

The SEM is an equipment that allows obtaining structural information of several samples. A high-energy thin beam of electrons focuses on the sample surface, in which, when interacting, a part of the beam is reflected and collected by a detector that converts this signal into a BSE image – backscattered electron image – or, in this interaction, the sample emits the electron, producing the SE (secondary electron) image. The emission of X-rays also occurs, providing the elementary chemical composition of a point or region of the surface, allowing the identification of practically any element present. The microscopic images were obtained using the SEM ZEISS, model EVO MA10 (Arcadia).

2.2.3. Adsorption thermodynamic – evaluation of the application potential of adsorbent carbon

Monocomponent adsorption equilibrium studies in batch reactor between the developed adsorbent and the metallic ions present in aqueous solution (Ni^{2+} , Cd^{2+} , Cu^{2+} , and Zn^{2+}), were performed at the temperatures of 23°C, 33°C, and 43°C \pm 1°C and at 150 rpm. 0.2 \pm 0.0001 g of adsorbent (best result obtained in preliminary tests) were added to nine Erlenmeyers of 100 mL. To conduct the equilibrium trials, the solutions were prepared with the pure components and distilled water in the following concentrations: 100, 90, 80, 70, 60, 50, 40, 30, and 20 mg L⁻¹, with pH adjusted at 5.5 \pm 0.1. The pH was chosen based on the solubility curve, concentration vs. pH for the metals studied. The equilibrium time was obtained in preliminary tests. All adsorption trials were performed in duplicate.

The number of metallic ions adsorbed in the equilibrium, q_e (mg g⁻¹), in each Erlenmeyer, was calculated by Eq. (3), obtained by a mass balance.

$$q_e = \frac{(C_0 - C_e) \times V}{w} \quad (3)$$

in which C_0 is the initial concentration (mg L⁻¹), C_e is the equilibrium concentration in the liquid phase (mg L⁻¹), V is the volume of the solution (L), and w is the adsorbent mass (g).

The concentration of solute in the liquid and solid phases in the solid and liquid interface can be related by an adsorption isotherm. The most used equilibrium isotherm models are presented in Table 1.

In which the Langmuir parameter b (L mg⁻¹) is a constant related to the adsorption energy or net enthalpy,

Table 1

Isotherm adsorption models of metallic ions in the developed adsorbent

Isotherms	Equations
Langmuir (Langmuir [65], Ruthven [32], Luz et al. [33], Shahbazi et al. [34])	$q_e = \frac{q_{\max} b_L C_e}{1 + b_L C_e}$ Eq. (4)
	$R_L = \frac{1}{1 + b_L C_e}$ Eq. (5)
Freundlich (Freundlich [66], Ruthven [32], Luz et al. [33], Shahbazi et al. [34])	$q_e = k_F C_e^{\frac{1}{n_F}}$ Eq. (6)

binding affinity of active sites [31]; q_{\max} (mg g⁻¹) is the maximum adsorption capacity on the monolayer; k_F (L g⁻¹) and n_F (dimensionless) are empirical Freundlich parameters, which depend on many experimental factors and they are related to the adsorption capacity and intensity of the adsorbent [32–36]. The Freundlich constant k_F indicates the adsorption bonding strength. The value of n_F is the heterogeneity factor that represents the distribution of the adsorption bonds and intensity [37].

To predict the favorability of the isotherm, the Langmuir parameters can be expressed in terms of a dimensionless separation factor, defined by Eq. (5). The isotherm is considered favorable when the Langmuir separation factor is between $0 < R_L < 1$, and the value of n_F is between $1 < n_F < 10$.

2.2.3.1. Temperature effect

The thermodynamic adsorption parameters, such as ΔH° (enthalpy variation) and ΔS° (entropy variation), will be calculated from the inclination and interception of the $\ln K_c$ vs. $1/T$ curves for the adsorption of metallic ions of the Jerivá coconut adsorbent, respectively, using the following relation:

$$\ln K_c = -\frac{\Delta H^\circ}{RT} + \frac{\Delta S^\circ}{R} \quad (7)$$

where ΔG° (free energy variation) will be calculated using the following relation:

$$\Delta G^\circ = \Delta H^\circ - T\Delta S^\circ \quad (8)$$

in which, R (8.314 J mol⁻¹ K⁻¹) is the constant of the gases, T (K) is the absolute temperature, and K_c (L mg⁻¹) is the thermodynamics equilibrium standard defined by $q_e C_e^{-1}$.

2.2.3.1. Non-linear regression analysis

In this work, all the parameters in the isotherm models were fit by non-linear regression using software STATISTICA 10. To compare and evaluate the better fit to the experimental data, between the Langmuir and Freundlich models, besides determining the coefficient (R^2), five different error functions were used. In each case, the isotherm parameters were determined by minimizing the respective error

function across the liquid-phase concentration range using the solver add-in with Microsoft’s spreadsheet Excel (Excel® software for Office 365 MSO 32 bits (Microsoft, USA).

The sum of the squares of the errors (ERRSQ), hybrid fractional error function (HYBRID), Marquardt’s percent standard deviation (MPSD), the average relative error (ARE), and the sum of the absolute errors (EABS) were obtained as follows [31,38]:

ERRSQ:

$$ERRSQ = \sum_{i=1}^p (q_{e,calc} - q_{e,meas})_i^2 \quad (9)$$

HYBRID:

$$HYBRID = \frac{100}{p-n} \sum_{i=1}^p \left[\frac{(q_{e,meas} - q_{e,calc})_i^2}{q_{e,meas}} \right]_i \quad (10)$$

MPSD:

$$MPSD = 100 \left(\sqrt{\frac{1}{p-n} \sum_{i=1}^p \left(\frac{q_{e,meas} - q_{e,calc}}{q_{e,meas}} \right)_i^2} \right) \quad (11)$$

ARE:

$$ARE = \frac{100}{p} \sum_{i=1}^p \left| \frac{q_{e,calc} - q_{e,meas}}{q_{e,meas}} \right|_i \quad (12)$$

EABS:

$$EABS = \sum_{i=1}^p |q_{e,calc} - q_{e,meas}|_i \quad (13)$$

where $q_{e,meas}$ is the observation from the batch experiment i ; $q_{e,calc}$ is the estimate from the isotherm; n is the number of observations in the experimental isotherm, and p is the number of parameters in the regression model. The smaller function value indicates the best curve fitting; however, due to the difference in scale among the error functions, it is necessary to normalize error functions (SNE) to perform it accurately [31].

3. Results and discussions

3.1. Adsorbent characterization

3.1.1. Physical characterization

The adsorbent used in this work was developed from the thermally treated Jerivá coconut (Fig. 1). The use of thermal treatment is justified by the mitigation of a few issues relative to the application of *in natura* lignocellulosic materials. According to Šoštarić et al. [28], the application of these *in natura* materials for adsorption processes presents additional disadvantages, such as low adsorption capacity and component release to the solution. Therefore, such materials must be subjected to activations. Thus, the soluble organic compounds are extracted, and the adsorption



Fig. 1. Jerivá coconut (*Syagrus romanzoffiana*).

performances are improved. To obtain a good adsorption performance, after drying and grinding, the adsorbent was carbonated and pyrolyzed at 500°C in a furnace for 2 h and 30 min (best result obtained in preliminary tests).

After carbonating and pyrolyzing the adsorbent, it was selected in a range of intermediate particle size of 60 mesh, which presented better adsorption results in the preliminary tests. The influence of the adsorbent particle size for adsorbing metallic ions was also studied by Sousa et al. [4], who verified an increase in the adsorption capacity as the particle size decreased. Similar results were found in this work.

After particle size classification, the physical characterization trials were conducted, during which 26.47% of volatile material (dry basis), low moisture (1.17% dry basis), low ash content (13.53% dry basis), and high fixed carbon content (58.83% dry basis) were found.

According to Grimwood and Ashman [35], the constituents of the coconut husk included approximately 29% of lignin, 23% of cellulose, and 26% of pectin and hemicellulose, in addition to 5% of inorganic matter and 26% of volatile material, such as water compounds. According to Luz et al. [33], the results of low moisture, low ash content, and high fixed carbon content demonstrate that this adsorbent can be qualified as a good material for the adsorption process.

According to Šoštarić et al. [28], the advantage of using lignocellulosic materials to treat water is that cellulose (which generally dominates the composition of these materials) presents good chemical stability and mechanical resistance due to its crystalline structure. However, cellulose has a limited number of hydroxyls available to bond with the metallic ions. This occurs because most of these groups are involved in the formation of a large number of inter and intramolecular hydrogen bonds.

3.1.2. Determination of functional groups

When a solid such as a carbonaceous material is submerged into water, it develops a charge on its surface from the dissociation of surface functional groups. This surface charge depends on the pH of the medium and the surface characteristics of the coal. The positive surface charge comes from the dissociation of acidic surface groups such as carboxylic and phenolic groups. The origin of the negative surface charge in coals without nitrogen groups is more uncertain, as it may come from basic oxygen groups, such as pyrones or chromenes, or from the existence of regions with high pi electrons in the graphemic layers, which act as a Lewis base. Thermal activation promotes basic groups on the surface of the adsorbent, as this procedure allows fixating oxygen in the active sites generated by the decomposition of carboxylic acids, lactones, and phenolic groups. These new oxygen-containing surface groups are basic, such as pyrone groups, which result from the combination of ether-type oxygen groups and the rest of the carbonyl groups [36].

In this work, the thermally treated adsorbent showed basic functional groups (9.58×10^{-4} m Eq g⁻¹) and acid surface groups (2.82×10^{-4} m Eq g⁻¹). Among the acid surface groups found, the activated carbon presented higher content of lactones (2.16×10^{-4} m Eq g⁻¹), carboxyl and phenolic groups (2.5×10^{-5} and 4.16×10^{-5} m Eq g⁻¹, respectively). Similar results were found by Zhu and Kolar [37], who studied the removal of p-cresol in coconut husk activated carbon. Further details regarding the functional groups present on the surface of the newly developed adsorbent can be seen in the results of the FTIR characterization.

3.1.3. Fourier transform infrared spectroscopy

Infrared spectroscopy allows identifying compounds in a sample due to the vibration of the molecules in a

certain number of waves [39]. The presence of functional groups such as C–O, C=O, C–H, and O=H is one of the main characteristics attributed to the presence of cellulose, hemicellulose, and lignin, characteristic of natural fibers [40].

Fig. 2 represents the infrared spectroscopy related to the sample of carbon material produced from the carbonation and pyrolysis of the *Syagrus romanzoffiana* fruits.

The most prominent characteristic of this spectrum is the presence of a wideband at 3,450.6 cm⁻¹. This region generally belongs to the elongation of the hydroxyl [41] –OH carboxyl and/or phenol [42] groups. It is known that the frequency region for bonds containing hydroxyl is found in the range of 3,800–2,700 cm⁻¹ [43].

The spike at 1,635.64 cm⁻¹ matches the presence of oxygenated (–C=O) and/or aromatic (–C=C–) (lignin) groups [39]. According to Baysal et al. [44] and Song et al. [45], they are generally found in the frequency between 1,600 and 1,850 cm⁻¹. The presence of aromatic groups (–C=C–) can also be reinforced by the presence of the aliphatic C–H group found in the spike at 2,956.87 cm⁻¹ (3,000–2,800 cm⁻¹) [45]. He et al. [41] evaluated the changes in physical properties of carbons, in which spikes in the frequency of 1,000–1,800 cm⁻¹ showed the presence of structures containing oxygen. Aliphatic structures are commonly found in the range of 2,800–3,000 cm⁻¹, and hydroxyls at 3,000–3,600 cm⁻¹ [45].

The spikes at 1,103.28 and 1,043.49 cm⁻¹ suggest the presence of ether, phenolic, and alcohol groups, which, according to literature, are present in spikes between 1,300 and 100 cm⁻¹ [45,46].

Thus, it is believed that the analysis conducted in the infrared spectrometer, using the Jerivá carbon, reflects the presence of the groups above mentioned, which can be reiterated and observed in the data found by Silverstein et al. [43].

The results obtained from the FTIR analysis reinforce those obtained in the determination of the surface

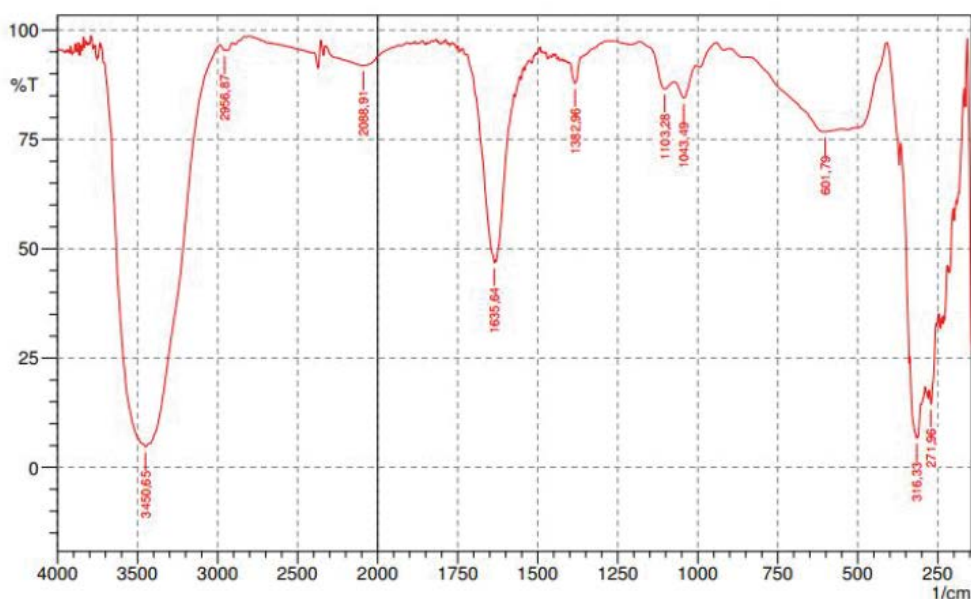


Fig. 2. Fourier transform infrared spectroscopy (FTIR) of the Jerivá coconut.

functional groups, which indicate the presence of basic and acid surface groups. The basic surface groups favor adsorption of metals, while acid surface groups, such as carbonylic, carboxylic, and phenolic, can develop a double layer on the surface of the adsorbent, also strengthening the adsorption of the studied metals.

3.1.4. Real density, pH_{pZC} and BET and BJH analyses

The real density of the material produced from Jerivá coconut was obtained by pycnometric analysis with helium gas, presented in Table 2, along with the results of BET and BJH area and charge point zero.

With the results obtained in the analysis of the density of the adsorbent material, it was possible to verify that it is very close to the densities obtained in studies using other materials. The activated carbon produced from Buriti seed, for example, presented real density of 1.759 kg m^{-3} [26]. Mohan and Gandhimathi [47] found an apparent density of 2.510 kg m^{-3} using steering ashes of carbon as adsorbent. Kumar et al. [48] found the apparent density of 740 kg m^{-3} for aerogel adsorbent.

For the point of zero charge analysis (pH_{pZC}), a value of 8.6 ± 0.1 was obtained. It is worth noting that this

parameter is extremely important, given that pH affects the adsorption of metallic ions. According to Appel et al. [49], the intensity of this effect can be higher or lower according to the charge of the surface of the adsorbent, which depends on its composition and characteristics. The pH_{pZC} represents the character of the studied carbon, which can be acid, basic, or neutral, presenting, in this case, acid character, with a predominance of positive charges on the surface of the adsorbent. Observing the good adsorption capacity of this adsorbent (Table 3), and compared with literature results (Table 5), it can be said that the positive charges of the metallic ions may be inducing some double layer adsorption on the surface of the adsorbent, which presents positive charges as well as negative charges that were generated by the thermal activation process.

The analysis of the structural property of the adsorbent includes the determination of the surface area, extension of the microporosity, and the distribution of the pore sizes. Fig. 3 represents the adsorption and desorption of nitrogen of the sample of the developed adsorbent.

By classifying the isotherms proposed by BET, the isotherm which represents the curve found in Fig. 3, by the adsorption of N_2 , is type II. The type II isotherm is characterized by the formation of multiple layers of adsorbate molecules on the surface of the solid. This type, known as BET, has been found in non-porous solid systems [32]. The result is justified due to the low particle size presented by the adsorbent developed in this work for the adsorption of heavy metals.

The measures of relative pressure and adsorbed volume of the N_2 gas are commonly used in many mathematical models to calculate the cover of N_2 monolayer adsorbed to the surface of the adsorbent. The BET model was applied to the N_2 adsorption data at the relative pressure of 0.05–1.00, when the cover of the N_2 molecule monolayer is assumed to be complete, obtaining the surface area of the activated carbon [32].

The results of the textural characterization of the adsorbent demonstrated good surface area ($107.57 \text{ m}^2 \text{ g}^{-1}$), with

Table 2
Results obtained for real density, BET and BJH area for the adsorbent produced from Jerivá coconut

Parameters	Values
Real density	$1,529.8 \text{ kg m}^{-3}$
pH_{pZC}	8.6 ± 0.1
Surface area	$107.57 \text{ m}^2 \text{ g}^{-1}$
Pore volume	$0.048 \text{ cm}^3 \text{ g}^{-1}$
Mean diameter of the pores	34.5 \AA
Pore internal area	$18.31 \text{ m}^2 \text{ g}^{-1}$
Pore distribution	$18\text{--}400 \text{ \AA}$

Table 3
Parameters of the Langmuir and Freundlich models

	$T \text{ (}^\circ\text{C)}$	Langmuir			Freundlich		
		$q_{\text{max}} \text{ (mg g}^{-1}\text{)}$	$b_L \text{ (L g}^{-1}\text{)}$	R^2	n_F	k_F	R^2
Cu^{2+}	23	16.01	0.85	0.89	12.12	11.32	0.87
	33	22.76	0.38	0.87	4.66	9.55	0.84
	43	25.08	0.30	0.90	0.22	10.27	0.85
Ni^{2+}	23	5.55	0.05	0.99	4.15	1.63	0.99
	33	29.07	0.07	0.87	2.12	3.15	0.61
	43	36.99	0.11	0.81	2.39	7.18	0.75
Cd^{2+}	23	16.38	0.34	0.98	4.52	6.69	0.96
	33	16.23	0.87	0.87	7.92	9.91	0.88
	43	16.50	0.90	0.90	14.65	13.12	0.91
Zn^{2+}	23	7.71	0.57	0.97	7.33	4.60	0.87
	33	8.01	0.74	0.74	11.40	7.90	0.74
	43	9.71	0.98	0.90	18.38	7.60	0.72

Table 4
Isotherm parameters with error analysis, method/error function (parameter set)

	Cobre (23°C) – Langmuir					Cobre (33°C) – Langmuir					Cobre (43°C) – Langmuir				
	ERRSQ	HYBRID	MPSD	ARE	EABS	ERRSQ	HYBRID	MPSD	ARE	EABS	ERRSQ	HYBRID	MPSD	ARE	EABS
q_{max}	15.49	15.24	15.00	14.30	15.09	22.7608	21.6765	20.7345	19.7361	19.7399	25.0840	24.5679	23.2547	25.0755	25.7681
b_L	0.99	0.80	0.69	0.76	1.21	0.3811	0.3966	0.4253	0.4320	0.4303	0.2985	0.2672	0.2935	0.1658	0.1590
ERRSQ	60.1183	62.5134	68.5055	77.6012	60.8744	158.347	164.287	177.868	204.569	204.674	146.636	151.905	166.585	196.964	190.295
HYBRID	54.0817	51.5994	53.4537	58.4521	54.5465	85.4587	81.6559	84.1237	93.8057	93.8731	93.3197	89.1709	92.4780	111.423	109.495
MPSD	40.9527	40.2115	40.0086	40.2039	41.0358	40.5697	39.9191	39.7581	40.0377	40.0444	43.1349	42.4426	42.2676	44.2293	44.2466
ARE	24.4685	23.9585	23.8956	23.7123	23.9869	24.6226	22.6384	21.6507	20.6314	20.6316	28.2628	27.1470	26.9282	25.2489	25.2089
EABS	19.6576	19.7328	20.3500	20.6528	19.0274	29.8753	27.0949	26.1445	25.2081	25.1999	30.4801	29.3682	30.1052	28.2810	27.7628
SNE	7.3952	7.3036	7.5062	7.8597	7.3595	7.4740	7.1680	7.2073	7.5043	7.5062	7.2572	7.0938	7.2739	7.7142	7.6092
Cobre (23°C) – Freundlich															
Cobre (33°C) – Freundlich															
Cobre (43°C) – Freundlich															
k_f	11.6231	10.4940	9.4944	11.9421	11.6836	9.5532	8.3255	7.6727	7.9496	7.9496	10.2655	8.2996	7.4416	7.4691	7.4822
n_f	14.9410	11.3862	9.2156	25.4366	17.2192	4.6588	4.1655	3.9528	4.5076	4.5076	4.6048	3.7324	3.4387	3.3995	3.4049
ERRSQ	67.4177	70.7243	79.5063	74.7545	68.4638	198.6680	208.5146	225.4782	265.6255	265.6254	205.040	220.823	242.052	237.347	237.062
HYBRID	63.9866	60.5951	63.4072	65.8839	62.9900	116.4268	107.1679	110.7224	126.1521	126.1521	127.982	110.855	115.219	114.022	113.926
MPSD	42.3010	41.2870	40.9850	42.1162	42.0586	43.9075	41.7467	41.3924	41.9554	41.9554	45.8742	41.9172	41.4293	41.4535	41.4543
ARE	25.5316	25.5007	25.6331	24.6564	25.1123	28.8792	26.3688	25.1360	24.3433	24.3433	29.9553	24.1129	22.4449	22.2674	22.2885
EABS	20.6414	21.5528	22.5867	20.2452	20.4080	33.2690	32.3610	32.0367	31.3702	31.3702	32.7307	28.2545	27.8767	27.2631	27.2681
SNE	15.3126	14.8343	14.7660	15.6834	15.3214	7.4585	7.1196	7.1720	7.5843	7.5843	7.7673	6.9866	7.0538	6.9758	6.9741
Cádmio (23°C) – Langmuir															
Cádmio (33°C) – Langmuir															
Cádmio (43°C) – Langmuir															
q_{max}	16.3763	15.6031	14.9922	15.7303	16.3162	16.5046	15.9968	16.2339	15.2164	15.2193	16.2339	15.6454	15.1212	13.9577	13.9579
b_L	0.3405	0.4643	0.5803	0.2573	0.2125	16.5172	18.9096	0.8738	23.3727	23.3553	0.8738	1.0201	1.1769	1.6342	1.6341
ERRSQ	41.3251	43.0163	47.3431	50.2733	48.6425	82.0632	84.0071	209.6101	94.6077	94.5506	55.8445	57.6263	62.3444	84.2926	84.2866
HYBRID	35.8789	34.2638	35.4592	42.6480	43.9972	49.3541	47.8229	177.9185	51.4509	51.4237	44.7855	43.3157	44.5325	56.5177	56.5140
MPSD	38.9984	38.5591	38.4440	39.6536	40.0493	38.7747	38.4575	50.7161	38.4691	38.4679	39.3552	38.9942	38.8876	39.4456	39.4454
ARE	22.2074	21.2608	20.5963	20.9418	21.2482	20.5907	19.3826	30.4940	18.0086	18.0103	23.1390	22.3631	21.7203	20.5026	20.5028
EABS	16.6399	16.0174	15.6921	15.3473	15.3950	18.6017	17.1957	30.8381	15.7755	15.7759	19.9680	19.4642	19.0780	18.4799	18.4800
SNE	7.3334	7.1783	7.2819	7.7371	7.7900	4.2902	4.1586	8.0000	4.1527	4.1521	5.1334	5.0594	5.1020	5.5860	5.5858
Cádmio (23°C) – Freundlich															
Cádmio (33°C) – Freundlich															
Cádmio (43°C) – Freundlich															
k_f	6.6923	7.1287	7.4832	8.6893	7.0016	13.1192	13.1416	13.0815	12.5896	12.9064	9.9133	9.9302	9.9271	9.9270	9.9271
n_f	4.5245	4.9853	5.4462	7.6898	4.7092	14.6458	17.0222	18.9065	19.5236	17.8123	7.9157	8.4264	11.5580	11.5579	11.5580
ERRSQ	18.4550	19.0641	20.7879	33.9555	18.8874	72.8925	75.0535	79.5154	92.2988	79.8067	49.1783	50.4294	82.5137	82.5139	82.5137
HYBRID	15.5316	15.0028	15.4695	23.3081	15.9969	46.3435	44.6736	45.6159	51.6308	45.8006	39.2478	38.2479	55.6503	55.6505	55.6503
MPSD	36.9168	36.7668	36.7221	37.1849	36.9535	38.7635	38.4200	38.3421	38.5933	38.3520	38.8424	38.5955	39.4064	39.4064	39.4064
ARE	17.6662	17.5308	17.4125	16.9581	17.5670	21.2331	20.2009	19.3679	18.5976	19.1937	22.6096	22.2003	20.4275	20.4275	20.4275

EABS	10.6265	10.7643	10.9095	11.2836	10.4443	19.3378	18.0564	17.0404	16.5534	16.8669	19.1140	18.9822	18.3564	18.3565	18.3564
SNE	6.5480	6.5255	6.6477	7.9198	6.5829	6.2795	6.1187	6.0967	6.3681	6.0845	13.4479	13.4179	14.7152	14.8782	14.8781
	Zinco (23°C) – Langmuir														
q_{\max}	6.5386	6.3669	6.2077	6.0000	6.5011	8.0163	7.1379	7.1379	7.8288	7.8862	11.8386	11.7353	11.8386	10.8880	10.8880
b_L	2,943.05	4,247.30	30,290.30	55,541.19	1,075.53	14.3969	47,211.7980	47,211.7980	15.5821	14.3911	0.4501	0.4474	0.4501	0.4908	0.4908
ERRSQ	6.9547	7.1295	7.6075	8.6881	6.9628	45.8035	51.7579	51.7579	46.0938	45.9524	7.1668	7.2322	7.1668	11.2191	11.2192
HYBRID	13.1882	12.8390	13.1354	14.4197	13.0525	98.3586	87.5265	87.5265	94.2860	95.4254	8.0412	7.9609	8.0412	11.5587	11.5589
MPSD	38.1806	37.9709	37.9075	38.0152	38.1223	58.0288	53.0278	53.0278	56.7415	57.1214	36.3835	36.3516	36.3835	36.6902	36.6903
ARE	18.8576	18.6249	18.4090	18.1277	18.8074	34.5415	33.4493	33.4493	33.8063	33.9804	16.1428	15.9777	16.1428	15.1686	15.1687
EABS	5.7253	5.7252	5.7250	5.7250	5.7258	15.5888	16.8019	16.8019	15.4680	15.4702	6.5244	6.4451	6.5244	6.0528	6.0529
SNE	5.9429	5.9141	5.9864	6.2215	5.9273	7.7535	7.6303	7.6303	7.6073	7.6431	4.7492	4.7227	4.7492	5.2180	5.2180
	Zinco (33°C) – Freundlich														
k_f	6.5375	6.3671	6.2052	5.0905	5.4702	7.9155	7.1375	7.1375	7.1350	7.8199	6.5164	6.1368	5.8140	7.1894	7.1016
n_f	1,565.825.66	477,651.10	95,825.74	28.43	50.55	330,956	330,956	330,956	330,956	330,956	7.0400	6.4234	5.9525	9.6978	9.3086
ERRSQ	6.9547	7.1289	7.6166	11.0545	9.9075	46.3150	51.7628	51.7628	51.7973	46.3972	10.4994	10.7667	11.4337	12.4121	12.0783
HYBRID	13.1840	12.8389	13.1442	18.2270	16.3415	97.0676	87.5269	87.5269	87.5270	94.8676	13.5192	13.0970	13.4149	16.2870	15.7706
MPSD	38.1789	37.9712	37.9076	38.6468	38.3261	57.4849	53.0265	53.0265	53.0163	56.8118	37.4108	37.2028	37.1455	37.9488	37.8504
ARE	18.8558	18.6251	18.4062	18.7354	18.4769	35.1592	33.4488	33.4488	33.4442	34.7347	18.2687	17.9782	17.9558	18.3189	18.2837
EABS	5.7250	5.7250	5.7252	6.2834	6.0448	16.2155	16.8024	16.8024	16.8048	16.1199	8.0469	8.0097	8.1978	7.9821	7.9737
SNE	4.6066	4.5839	4.6244	5.2725	5.0303	7.8047	7.6274	7.6274	7.6281	7.7202	5.0574	5.0143	5.0881	5.3603	5.3016
	Níquel (23°C) – Langmuir														
q_{\max}	5.5547	5.4666	5.3707	5.7687	5.7770	25.9034	24.9881	23.4049	22.4485	22.4404	208.2664	75.3702	18.2749	37.0751	78.6953
b_L	0.0657	0.0695	0.0740	0.0646	0.0644	0.0552	0.0496	0.0522	0.0539	0.0539	0.0080	0.0187	0.1485	0.0410	0.0299
ERRSQ	0.3282	0.3313	0.3421	0.4373	0.4411	235.4044	246.9035	265.9863	282.9464	283.0404	1,788.4598	2,467.4181	4,115.2945	3265.8437	1,813.4237
HYBRID	1.0174	1.0092	1.0197	1.4013	1.4135	125.4887	115.4216	119.0345	124.9860	125.0221	1,281.7558	909.3038	1,164.7175	990.2535	1,301.4736
MPSD	35.7128	35.7046	35.7014	35.8598	35.8641	43.7144	41.7768	41.4968	41.6082	41.6091	112.0495	78.2864	67.1106	69.5460	114.1840
ARE	12.4468	12.4913	12.5484	11.9001	11.8941	28.7836	24.5813	23.3484	22.5788	22.5744	68.7126	59.7918	55.0768	55.2016	67.8422
EABS	1.0136	1.0460	1.0853	0.7443	0.7403	32.3608	28.5022	27.4012	26.7179	26.7138	101.1589	120.8680	145.2428	129.6781	99.7300
SNE	6.9599	6.9958	7.0945	7.5521	7.5779	7.4786	6.9515	6.9860	7.0951	7.0957	6.7411	6.0292	6.9805	6.3147	6.7656
	Níquel (43°C) – Langmuir														
k_f	1.6260	1.6541	1.6898	1.6707	1.6670	4.0106	3.0345	2.7174	2.6399	2.8196	2.3563	2.2823	3.8125	5.8992	5.8321
n_f	4.1507	4.2383	4.3516	4.2012	4.1927	2.5448	2.2320	2.1477	2.2173	2.2865	1.1970	1.3698	2.3376	6.2215	1.8772
ERRSQ	0.2462	0.2475	0.2524	0.2683	0.2674	262.6110	276.7973	295.6677	344.1229	333.0790	1,780.2912	2,462.5512	3,991.5014	5,332.7133	1,853.6353
HYBRID	0.7613	0.7578	0.7626	0.8483	0.8456	143.0658	128.1657	131.8395	151.9532	146.5440	1,278.9447	900.1488	1,134.8361	1,508.7536	1,308.8702
MPSD	35.6221	35.6186	35.6172	35.6582	35.6572	45.6456	42.2876	41.8996	42.6310	42.3671	112.0443	77.3572	66.4887	70.8976	114.9968
ARE	12.0777	12.1345	12.1980	11.7188	11.7160	32.1665	26.2014	23.8371	22.1819	22.3883	67.6740	58.4992	53.5221	53.3278	73.7971
EABS	0.8592	0.8909	0.9270	0.6942	0.6935	35.5084	31.2493	29.6412	28.4393	28.2220	100.3341	120.2115	142.3164	162.3045	105.6279
SNE	7.5768	7.6194	7.7076	7.6703	7.6580	7.3289	6.6585	6.5979	6.9552	6.8385	6.0336	5.3333	6.0235	7.0618	6.3230

Table 5
Comparison of some heavy metals adsorbed on various adsorbents material from a natural source

Adsorbent	Modifying agent (s)	Heavy metal	Temperature (K)	C_0 (mg L ⁻¹)	q_{max} (mg g ⁻¹)	Source
Apricot husks	Alkaline pre-treatment NaOH	Pb ²⁺	323	6–120	22.19	[28]
		Zn ²⁺			5.06	
		Cu ²⁺			4.24	
Buriti fibers	Alkaline pre-treatment NaOH	Cd ²⁺	301	100–500	635.00	[55]
		Ni ²⁺			159.62	
		Cu ²⁺			153.75	
Coconut husk	No treatment	Cu ²⁺	293	100–500	443.0	[18]
		Ni ²⁺			404.5	
		Zn ²⁺			338.0	
Mustard peel	No treatment	Cd ²⁺	293	1–5	42.85	[56]
Cellulosic waste orange peel	No treatment	Cu ²⁺	293	10–40	63.30	[59]
Cashew nut shells	No treatment	Cu ²⁺	303	10–50	20.0	[57]
		Ni ²⁺		10–50	18.9	[59]
Coconut shells	NaOH and H ₂ SO ₄	Cr ²⁺	303	5–300	18.7	[62]
Corncob	No treatment	Cu ²⁺	303	5–300	19.9	[63]
Orange peel	Grafted copolymer	Cd ²⁺	298	5–120	5.1	[63]
		Ni ²⁺			293	50–1,200
Lemon peel	No treatment	Cu ²⁺	303	100–800	70.92	[64]
		Pb ²⁺			37.87	
		Zn ²⁺			27.86	
		Ni ²⁺			80.00	
		Cd ²⁺			54.64	

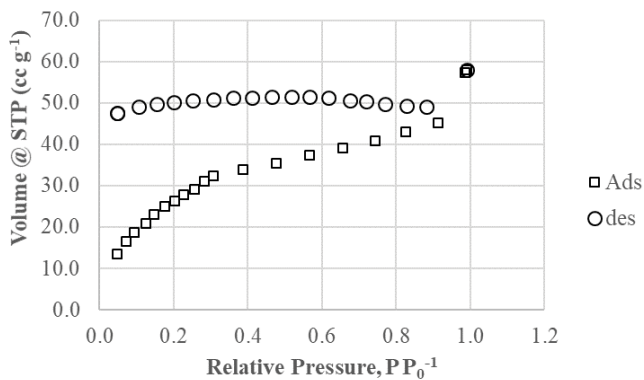


Fig. 3. N₂ adsorption and desorption isotherm for Jerivá coconut activated carbon.

pore distribution between the minimum value of 18 Å and the maximum value of 400 Å, presenting most pores between 20 and 50 Å. Singh and Balomajumder [50] found a surface area of 81.82 m² g⁻¹ in coconut husk activated carbon, stating that, for this value, the surface area of the material can be used as an adsorbent. Šoštarčić et al. [28] found a surface area of 15.4 m² g⁻¹ for native apricot husk and 20.4 m² g⁻¹ for apricot husk treated with alkali. Alves et al. [51] found a surface area of 754 m² g⁻¹ for adsorbent from the babassu epicarp and mean pore size (20.79 Å). In this case, it was possible to remove micropollutants of a real matrix from the public water supply. Therefore, with the results obtained for BET, BJH, and real density, it is possible to verify the potential to apply the developed material in the adsorption processes of contaminated water.

3.1.5. Scanning electron microscopy

The images of the activated carbon surface were obtained using SEM, in the magnifications of 250; 507; 1,070; and 2,000 times, and they are presented in Fig. 4. In Fig. 4, it is possible to verify a rough surface, confirming the results of the structural characterization, in which the distribution of pore sizes ranged from 20 to 50 nm, with a predominance of mesopores (intermediate diameter of approximately 34.5 nm).

3.2. Adsorption thermodynamic equilibrium

The adsorption equilibrium provides fundamental information to elucidate the applicability of the adsorption process [52]. The adsorption study was conducted with the objective of determining the maximum adsorption capacity of metallic ions by the developed adsorbent and evaluating its efficiency. The time consumed until reaching the equilibrium between the solution compounds and the adsorbent was obtained in preliminary tests (30 min), with similar results found by Malik et al. [18], who studied the adsorption of copper, nickel, lead, and zinc in aqueous solution using coconut husk adsorbent.

The initial pH of adsorption for all metals studied in the monocomponent solution was 5.5 ± 0.1 . After the adsorption equilibrium experiments, the pH found for the studied metals were: 6.9 ± 0.1 for Cu^{2+} , 7.3 ± 0.1 for Cd^{2+} , 7.6 ± 0.1 for Ni^{2+} , and 7.3 ± 0.1 for Zn^{2+} . These results are consistent as the point of zero of charge found for this adsorbent was 8.6 ± 0.1 . This high value of pH_{PCZ} causes an increase in the pH of the solution after equilibrium. This same behavior was observed in Liu et al. [53] and Huang et al. [54].

Therefore, the number of contaminants removed per mass unit of the adsorbent solid was determined by Eq. (3). All results experimentally obtained for adsorption equilibrium of metallic ions Cu^{2+} , Ni^{2+} , Cd^{2+} , and Zn^{2+} in the temperatures of 23°C, 33°C, and 43°C were adjusted using the minimum square method of software STATISTICA 10, according to the Langmuir and Freundlich models (Table 1). The values of b_L (L mg^{-1}), q_{max} (mg g^{-1}), k_F (L g^{-1}), n_F (dimensionless), and respective determination coefficient (R^2) were calculated considering the 95% confidence level, and they are shown in Table 3.

The approach of determination of the isotherm parameters for the four metallic ions by nonlinear regression appears to give acceptable fits to the experimental data with respective regression coefficients (R^2 values) close

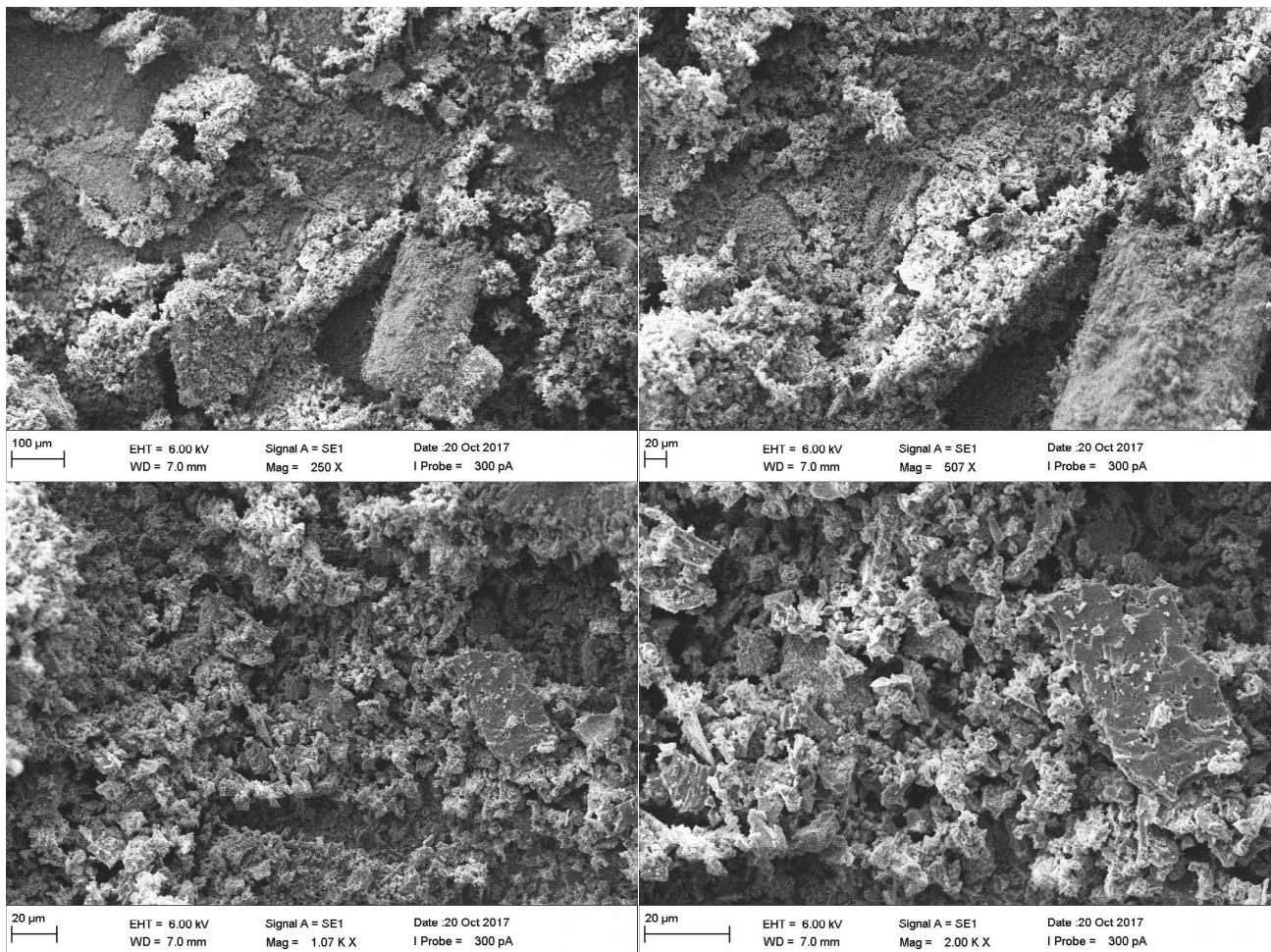


Fig. 4. Scanning electron microscopy in the magnifications of 250; 507; 1,070; and 2,000 times.

to unity, as shown in the Tables 3. Overall, the Langmuir model the highest R^2 values, whereas the Freundlich values are considerably lower. The values of R^2 indicate that the Langmuir isotherm model obtained better fit to the experimental data (R^2 varying between 0.89 and 0.99). But comparison for better fit to the experimental data, between the Langmuir and Freundlich models using only R^2 is not sufficient. Therefore, a statistical analysis was also performed using different error functions, which indicated the significance between the Langmuir and Freundlich models. The parameter sets were determined by nonlinear regression using the five different error functions as detailed earlier. The process of minimizing the respective error functions across the experimental concentration ranges examined yields the isotherm parameters. The isotherm parameters so obtained, along with the values of the error measures for each isotherm and the final sum of the normalized error values (SNE), are presented in full in Table 4.

A comparison of the scaled errors can be undertaken, and hence, identification can be made of the isotherm constants, which would provide the closest fit to the measured data.

The comparison and analysis of the parameters of the isotherms that best fit the experimental data were made with a view to the data sets presented in Table 4. For Cu^{2+} ion, the lowest normalized error values (SNE) at 23°C and 33°C were better approximated by HYBRID; and at 43°C by EABS. At 23°C, the lowest SNE was obtained from Langmuir isotherm parameters and at 33°C and 43°C, the SNE is close to and within the 95% confidence interval, that is, within the error range of 5% for both models studied. Thus, the parameters that best approximate the experimental data of the metallic ion Cu^{2+} at temperatures 33°C and 43°C are the parameters obtained from the parameters of both Langmuir and Freundlich isotherms; and at 23°C they are based on Langmuir isotherm parameters.

At temperatures of 23°C and 43°C the metallic ions Cd^{2+} and Zn^{2+} presented lower SNE for HYBRID and at 33°C for EABS and ARE, respectively. Despite being close to 23°C, the lowest values were based on the Freundlich isotherm parameters. At 33°C and 43°C the SNE of Cd^{2+} was lower from Langmuir isotherm parameters. The SNE of Zn^{2+} at 33°C and 43°C are within the 95% confidence level, so the parameters that best approximate the experimental data are both Langmuir and Freundlich isotherms.

The metallic ion Ni^{2+} demonstrates lower SNE values at 23°C for ERRSQ, 33°C for MPSD, and 43°C for HYBRID. The SNE at 43°C from the Langmuir and Freundlich isotherm parameters, although close, the lowest SNE was found from the Freundlich isotherm parameters. On the other hand, the differences between the SNE at 23°C and 33°C are within the 5% error range, indicating that the parameters that best approximate the experimental data of Ni^{2+} may be Langmuir and Freundlich isotherms.

Therefore, at 33°C and 43°C, the parameters that best approximate the experimental data of the metallic ion Cu^{2+} are from both Langmuir and Freundlich models, for Cd^{2+} the Langmuir model and for Zn^{2+} for both Langmuir and Freundlich models. At 23°C, Cu^{2+} was best approximated by the Langmuir model for Cd^{2+} and Zn^{2+} by the Freundlich model. The metallic ion Ni^{2+} at 23°C and 33°C, both Langmuir

and Freundlich models and at 43°C, was better approximated by the Freundlich model.

Figs. 5a–d show the results of the experimental adsorption isotherms for the studied metals, presenting the best result of the adjustments, obtained by the Langmuir model from minimum errors calculated and shown in Table 4.

Considering that the temperature of 43°C presents the best adsorption of metallic ions Cu^{2+} , Ni^{2+} , Cd^{2+} , and Zn^{2+} , it was observed by regression coefficients (R^2 values) that the Langmuir isotherm was the model that best fit the experimental data. On the other hand, by analyzing the five error functions shown in Table 4, for the ions Cu^{2+} and Zn^{2+} , both Langmuir and Freundlich isotherms fit well with the experimental data, and for Cd^{2+} Langmuir's isotherm model and for Ni^{2+} Freundlich's isotherm model presented a better fit, respectively. The adsorption of ions Cu^{2+} , Ni^{2+} , Cd^{2+} , and Zn^{2+} by the developed adsorbent demonstrated that the Langmuir isotherm model obtained better fit to the experimental data, with R^2 varying between 0.89 and 0.99.

The data of the dimensionless separation factor, commonly known as Langmuir parameter R_L , ranged from 0.01 to 0.54, indicating favorable adsorption for all studied metallic ions. The Freundlich parameter n_F revealed no favorable adsorption for any of the studied metallic ions ($1 < n_F < 10$).

Regarding the temperature with higher adsorption capacity, it can be seen in Tables 3 and 4 that q_{max} has the highest value for the temperature of 43°C. Similarly, it can also be checked via k_F except for Cu^{2+} . The maximum adsorption capacity is an important characteristic to know the performance of the adsorbent. The adsorption of the studied metallic ions with the developed adsorbent was endothermic. The parameters demonstrated in Table 4 show a better adsorption capacity for Ni^{2+} (36.99 mg g⁻¹), followed by Cu^{2+} (25.08 mg g⁻¹), Cd^{2+} (16.50 mg g⁻¹), and Zn^{2+} (9.71 mg g⁻¹), for the highest temperature studied (43°C).

Table 5 presents some literature results of the metallic ions adsorption under adsorbents obtained from natural source raw material, showing the maximum adsorption capacity for some metals under certain experimental conditions.

Through Table 5, we verify that Šoštarić et al. [28] found a maximum adsorption capacity for metallic ions of 22.19 mg g⁻¹ for Pb^{2+} , 5.06 mg g⁻¹ for Zn^{2+} , and 4.24 mg g⁻¹ for Cu^{2+} when studying alkali-treated apricot husks at a temperature of 50°C. de Melo et al. [55] demonstrated a maximum adsorption capacity for metallic ions of Cd^{2+} (635.00) > Ni^{2+} (159.62) > Cu^{2+} (153.75) mg g⁻¹ using buriti fibers subjected to an alkaline pre-treatment at a temperature of 28°C (initial metallic ions concentration was 100–500 mg L⁻¹). Studies conducted by Malik et al. [18] demonstrated a maximum adsorption capacity of metallic ions of 443 mg g⁻¹ for Cu^{2+} , 404.5 mg g⁻¹ for Ni^{2+} , and 338 mg g⁻¹ for Zn^{2+} , for the coconut husk adsorbent. According to these authors, who used the initial concentrations from 100 to 500 mg L⁻¹ of the metallic compounds, the maximum adsorption capacity increases according to the increase in concentration of adsorbate and adsorbent mass, increasing the motor strength for transportation. The studies conducted by Meena et al. [56] demonstrated maximum adsorption capacity for the Cd^{2+} ion in the mustard peel of 42.85 mg g⁻¹. Guiza [57] obtained maximum adsorption capacity for Cu^{2+} in Orange peels of 63.30 mg g⁻¹. Feng et al. [58] performed an orange peel

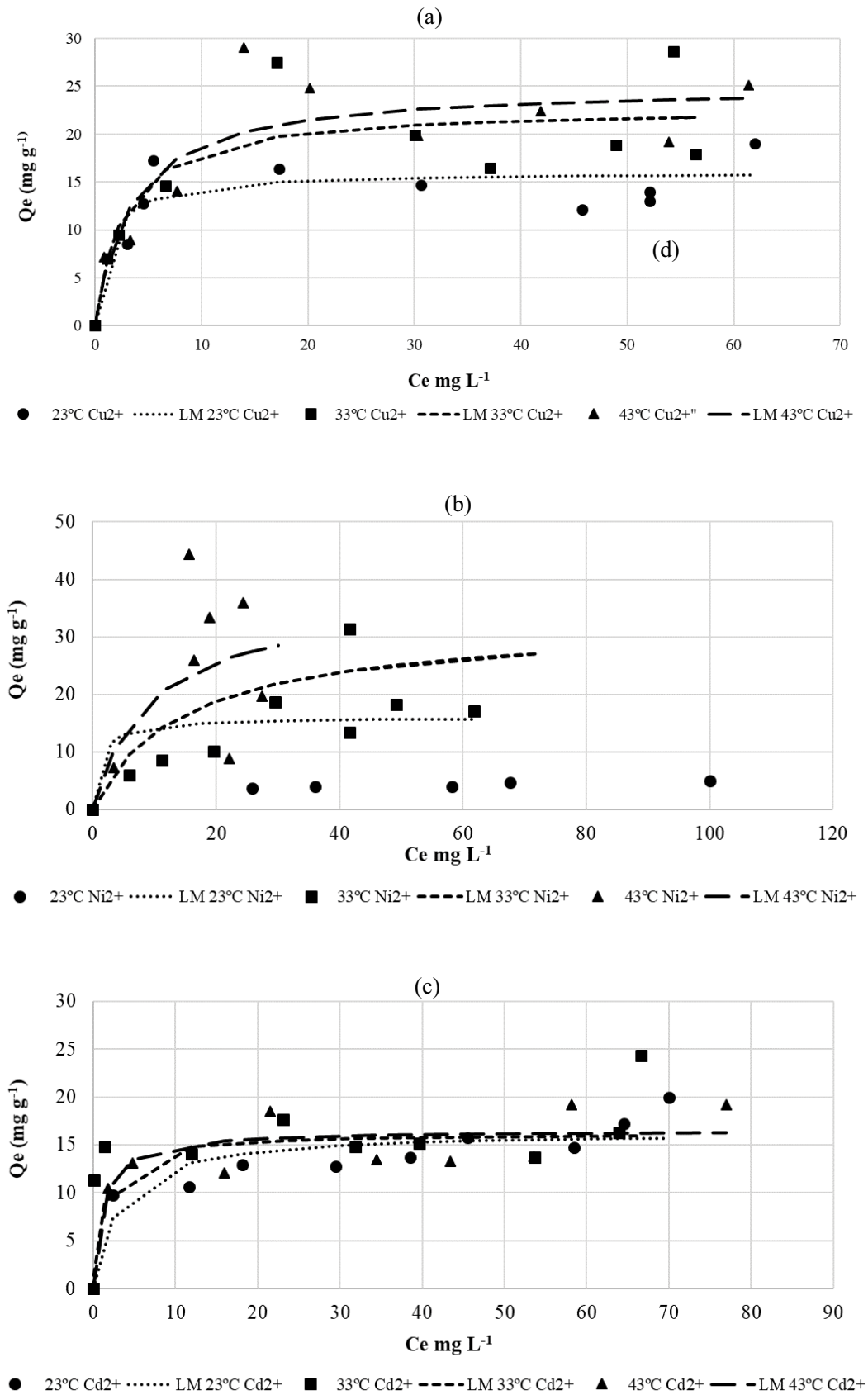


Fig. 5. (Continued)

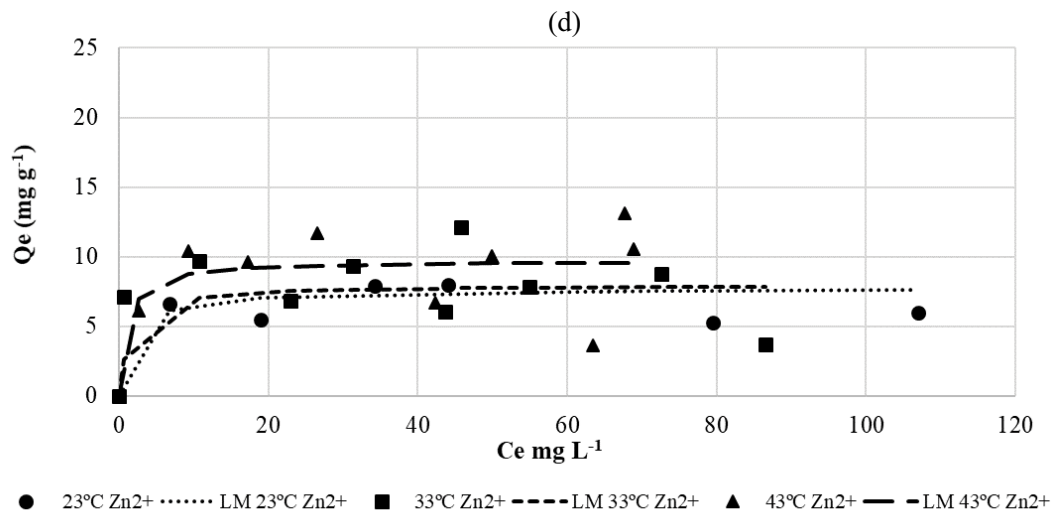


Fig. 5. Adsorption isotherm of the metallic ions in aqueous solution using the developed adsorbent: (a) Cu^{2+} , (b) Ni^{2+} , (c) Cd^{2+} , and (d) Zn^{2+} . The best adjusted isothermal parameters; Temperatures of 23°C, 33°C, and 43°C ($\pm 1^\circ\text{C}$); $w = 0.2 \pm 0.0001$ g; $\text{pH} = 5.5 \pm 0.1$; 150 rpm.

polymeric treatment for the adsorption of Cd^{2+} and Ni^{2+} ions, achieving maximum capacities in the order of 292.3 and 162.6 mg g^{-1} , respectively. The studies of Kumar et al. [59,60] revealed a maximum adsorption capacity of 20.00 and 18.89 mg g^{-1} for adsorbent made from cashew nut shells without any chemical modification in the removal of metallic ions Cu^{2+} and Ni^{2+} , respectively. Acid and alkaline modified coconut shells were also used in the adsorption of Cr^{2+} (18.7 mg g^{-1}) [61] and Cu^{2+} (19.9 mg g^{-1}) [62]. Leyva-Ramos et al. [63] investigated the application of corncobs to remove Cd^{2+} at concentrations ranging from 5 to 120 mg L^{-1} , finding 5.1 mg g^{-1} as maximum adsorption capacity. The study of Thirumavalavan et al. [64] demonstrated that lemon peels can be used to remove metallic ions since the authors have been able to obtain significant adsorption capacities for different metals such as Cu^{2+} (70.92 mg g^{-1}), Pb^{2+} (37.87), Zn^{2+} (27.86 mg g^{-1}), Ni^{2+} (80.00 mg g^{-1}), and Cd^{2+} (54.64 mg g^{-1}).

3.2.1. Effect of temperature

Fig. 6 shows the $\ln K_c$ plot vs. $1/T$ of the studied metals under the carbon obtained from the Jerivá coconut. It was

verified that the adsorption of the metallic ions increases according to the increase in temperature (from 23°C to 43°C). The increase in adsorption capacity proportionate to temperature indicates an endothermic process. The increase in adsorption may be attributed to either increase in the number of active surface sites available for adsorption on the adsorbent or the desolvation of the adsorbing species and the decrease in the thickness of the boundary layer surrounding the adsorbent with temperature, so that the mass transfer resistance of the adsorbate in the boundary layer decreases. At higher temperatures, the possibility of solute diffusion within the pores of the adsorbent may not be overlooked. Since diffusion is an endothermic process, greater adsorption will be observed at higher temperatures [57]. Thus, the diffusion rate of ions in the external mass transport process increases with temperatures. The results demonstrated above were further substantiated by the various adsorption thermodynamic parameters evaluated (Table 3).

The adsorption thermodynamic parameters such as ΔH° (enthalpy variation) and ΔS° (entropy variation) were determined with the inclination and interception of the Vant Hoff graphic vs. $1/T$ (Fig. 6).

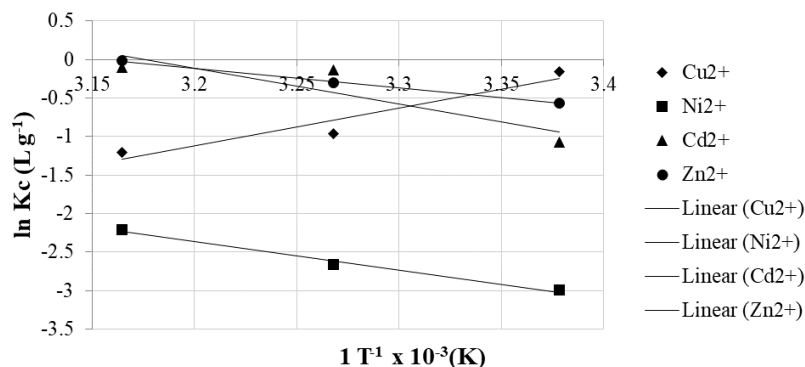


Fig. 6. Vant Hoff graphic of the adsorption of metallic ions.

Table 6 presents the thermodynamic parameters ΔH° , ΔS° , and ΔG° for the adsorption of metallic ions under the developed adsorbent. It is possible to verify that Ni^{2+} , Cd^{2+} , and Zn^{2+} presented positive ΔH° values, indicating that the adsorption process is endothermic, while Cu^{2+} obtained negative value, indicating an exothermic process. The endothermic process can also be confirmed by observing the results of the maximum adsorption capacity (q_{max}) in Table 4, which increases according to the increase in solution temperature.

The results for ΔS° were positive for Ni^{2+} , Cd^{2+} , and Zn^{2+} , indicating adsorbent affinity. The negative sign for Cu^{2+} can be related to the decrease in the degree of freedom of the solid/liquid interface during adsorption. The results for ΔG° were negative for Ni^{2+} , Cd^{2+} , and Zn^{2+} , which indicates a spontaneous adsorption process for the three metallic ions evaluated at different temperatures, with the exception of Cu^{2+} .

Therefore, the results presented in this work, that the increase in temperature (23°C to 43°C) increases the adsorption process of metallic ions using Jerivá coconut adsorbent, was also verified for other adsorbents in the literature. In the same manner as Liu et al. [53] the adsorption of ions Cu^{2+} , Ni^{2+} , and Zn^{2+} in the temperatures of 30°C, 60°C, and 80°C, and as Malik et al. [18], in the removal of ions Cd^{2+} , Pb^{2+} , Hg^{2+} , Cu^{2+} , Ni^{2+} , Mn^{2+} , and Zn^{2+} , in the temperatures of 20°C and 30°C.

4. Conclusions

The new adsorbent developed from the Jerivá coconut presents good characteristics for the adsorption of metallic ions of synthetic water, with promising application variability in water supply and effluent treatment.

The greatest adsorption capacity occurs for Ni^{2+} , followed by Cu^{2+} , Cd^{2+} , and Zn^{2+} . The results of the characterization analyses of the developed adsorbent show that the basic surface groups favor the adsorption of the metals

and that the acid surface groups strengthen the adsorption of the studied metals. In the pH_{PZC} study, it was verified, predominance of positive charges on the surface of the adsorbent, and that along with the negative charges caused by the thermal activation process, they may be promoting double-layer adsorption.

It was possible to verify the potential for application of the developed adsorbent in adsorption processes by means of the surface area ($107.57 \text{ m}^2 \text{ g}^{-1}$) and real density ($1,529.8 \text{ kg m}^{-3}$).

The adsorption was strongly influenced by temperature. The increase in adsorption along with temperature can be attributed to an increase in the number of active surface locations available for adsorption in the adsorbent or in the desolvation of the chemical species, and in the decrease of the thickness of the limit layer surrounding the adsorbent with the temperature, for the transfer mass resistance of the adsorbate in the limit layer to decrease. The thermodynamic parameters, such as ΔH° , ΔS° , and ΔG° confirm the endothermic, spontaneous, and favorable adsorption of ions Ni^{2+} , Cd^{2+} , and Zn^{2+} , and non-spontaneous for ion Cu^{2+} .

The values of the isothermal parameters b , q_{max} , k_F , and n_F were calculated considering 95% confidence level, analyzed by the value of the determination coefficient (R^2) and statistical analysis using different error functions to minimize.

It can be concluded that Langmuir isotherm is a model that closely approximates experimental data, and Freundlich isotherm is a model that approximates experimental data at some temperatures. That is, the Langmuir model best fitted the experimental adsorption data of the metallic ions Cu^{2+} at 23°C, 33°C, and 43°C, Cd^{2+} at 33°C and 43°C, Zn^{2+} at 33°C and 43°C, Ni^{2+} at 23°C and 33°C; and the Freundlich model best fitted the experimental adsorption data of the metallic ions Cu^{2+} at 33°C and 43°C, Cd^{2+} at 23°C, Zn^{2+} at 23°C, Ni^{2+} at 23°C, 33°C, and 43°C.

When compared to other adsorbents presented in the literature, the Jerivá coconut adsorbent presented good efficiency in the removal of toxic metals. Therefore, it has great application potential for the treatment of water.

Acknowledgments

The authors thank the Federal University of Fronteira Sul – UFFS, campus Erechim, and the Fundação Universidade do Estado de Santa Catarina – UDESC Oeste – SC, for the infrastructure yielded for the development of the research.

Funding

This work was supported by CAPES, FAPESC, and Fundação Universidade do Estado de Santa Catarina – UDESC Oeste – SC [grant number 01].

References

- [1] O.E. Abdel Salam, N.A. Reiad, M.M. El-Shafei, A study of the removal characteristics of heavy metals from wastewater by low-cost adsorbents, *J. Adv. Res.*, 2 (2011) 297–303.
- [2] Environmental Brazilian Laws, Portaria do Ministério da Saúde, Diário Oficial da União, seção 3, Portaria n° 5, 2017.
- [3] H. Tounsadi, A. Khalidi, A. Machrouhi, M. Farnane, R. Elmoubaraki, A. Elhalil, M. Sadiq, N. Barka, Highly efficient activated carbon from *Glebionis coronaria* L. biomass: optimization of

Table 6
Thermodynamic parameters for the adsorption of metallic ions adsorbed in the Jerivá coconut

	Thermodynamic parameters			
	T (K)	ΔG° (kJ mol ⁻¹ K ⁻¹)	ΔH° (kJ mol ⁻¹)	ΔS° (kJ mol ⁻¹ K ⁻¹)
Cu^{2+}	296	41.29		
	306	42.73	-0.04	-0.14
	316	44.08		
Ni^{2+}	296	-23.13		
	306	-23.92	0.03	0.08
	316	-24.70		
Cd^{2+}	296	-35.87		
	306	-37.09	0.04	0.12
	316	-38.30		
Zn^{2+}	296	-19.63		
	306	-20.30	0.02	0.07
	316	-20.96		

- preparation conditions and heavy metals removal using experimental design approach, *J. Environ. Chem. Eng.*, 4 (2016) 4549–4564.
- [4] F.W. Sousa, S.A. Moreira, A.G. Oliveira, R.M. Cavalcante, R.F. Nascimento, M.F. Rosa, Uso da casca de coco verde como adsorbente na remoção de metais tóxicos, *Quim. Nova*, 30 (2007) 1153–1157.
- [5] E. Menya, P.W. Olupot, H. Storz, M. Lubwama, Y. Kiros, Production and performance of activated carbon from rice husks for removal of natural organic matter from water: a review, *Chem. Eng. Res. Des.*, 129 (2018) 271–296.
- [6] J.M.V. Nabais, C.E.C. Laginhas, P.J.M. Carrott, M.M.L. Ribeiro Carrott, Production of activated carbons from almond shell, *Fuel Process. Technol.*, 92 (2011) 234–240.
- [7] J. Zhou, Y. Liu, X. Zhou, J. Ren, C. Zhong, Magnetic multiporous bio-adsorbent modified with amino siloxane for fast removal of Pb(II) from aqueous solution, *Appl. Surf. Sci.*, 427 (2018) 976–985.
- [8] I.P.d.P. Cansado, C.R. Belo, P.A.M. Mourão, Valorisation of *Tectona grandis* tree sawdust through the production of high activated carbon for environment applications, *Bioresour. Technol.*, 249 (2018) 328–333.
- [9] M. Wiśniewska, P. Nowicki, A. Nosal-Wiercińska, Adsorption of poly(acrylic acid) on the surface of microporous activated carbon obtained from cherry stones, *Colloids Surf., A*, 514 (2017) 137–145.
- [10] S. Hokkanen, A. Bhatnagar, M. Sillanpää, A review on modification methods to cellulose-based adsorbents to improve adsorption capacity, *Water Res.*, 91 (2016) 156–173.
- [11] A.P. Vieira, S.A.A. Santana, C.W.B. Bezerra, H.A.S. Silva, J.C.P. de Melo, E.C. da Silva Filho, C. Airoidi, Copper sorption from aqueous solutions and sugar cane spirits by chemically modified babassu coconut (*Orbignya speciosa*) mesocarp, *Chem. Eng. J.*, 161 (2010) 99–105.
- [12] K. Björklund, L.Y. Li, Adsorption of organic stormwater pollutants onto activated carbon from sewage sludge, *J. Environ. Manage.*, 197 (2017) 490–497.
- [13] S. Babel, T.A. Kurniawan, Low-cost adsorbents for heavy metals uptake from contaminated water: a review, *J. Hazard. Mater.*, 97 (2003) 219–243.
- [14] S.K. Hubadillah, M.H.D. Othman, Z. Harun, A.F. Ismail, M.A. Rahman, J. Jaafar, A novel green ceramic hollow fiber membrane (CHFM) derived from rice husk ash as combined adsorbent-separator for efficient heavy metals removal, *Ceram. Int.*, 43 (2017) 4716–4720.
- [15] Suhas, V.K. Gupta, P.J.M. Carrott, R. Singh, M. Chaudhary, S. Kushwaha, Cellulose: a review as natural, modified and activated carbon adsorbent, *Bioresour. Technol.*, 216 (2016) 1066–1076.
- [16] B. Tiryaki, E. Yagmur, A. Banford, Z. Aktas, Comparison of activated carbon produced from natural biomass and equivalent chemical compositions, *J. Anal. Appl. Pyrolysis*, 105 (2014) 276–283.
- [17] P.R. Aranda, I. Llorens, E. Perino, I. De Vito, J. Raba, Removal of arsenic(V) ions from aqueous media by adsorption on multiwall carbon nanotubes thin film using XRF technique, *Environ. Nanotechnol. Monit. Manage.*, 5 (2016) 21–26.
- [18] R. Malik, S. Dahiya, S. Lata, An experimental and quantum chemical study of removal of utmostly quantified heavy metals in wastewater using coconut husk: a novel approach to mechanism, *Int. J. Biol. Macromol.*, 98 (2017) 139–149.
- [19] F.Q. An, R.Y. Wu, M. Li, T.P. Hu, J.F. Gao, Z.G. Yuan, Adsorption of heavy metal ions by iminodiacetic acid functionalized D301 resin: kinetics, isotherms and thermodynamics, *React. Funct. Polym.*, 118 (2017) 42–50.
- [20] M.A.C. Moreira, M.E. Payret Arrúa, A.C. Antunes, T.E.R. Fiuza, B.J. Costa, P.H. Weirich Neto, S.R.M. Antunes, Characterization of *Syagrus romanzoffiana* oil aiming at biodiesel production, *Ind. Crops Prod.*, 48 (2013) 57–60.
- [21] S.L. Falasca, C.M. del Fresno, A. Ulberich, Possibilities for growing queen palm (*Syagrus romanzoffiana*) in Argentina as a biodiesel producer under semi-arid climate conditions, *Int. J. Hydrogen Energy*, 37 (2012) 14843–14848.
- [22] M.C. Coimbra, N. Jorge, Proximate composition of guariroba (*Syagrus oleracea*), jerivá (*Syagrus romanzoffiana*) and macaúba (*Acrocomia aculeata*) palm fruits, *Food Res. Int.*, 44 (2011) 2139–2142.
- [23] INMETRO, Orientação Sobre Validação de Métodos Analíticos, DOQ – CGCRE, 2018, Brasil, p. 28.
- [24] Associação Brasileira de Normas Técnicas (ABNT), NBR 10664 Águas – Determinação de Resíduos (Sólidos), Satandard n° 10664, 1989.
- [25] H.P. Boehm, Some aspect of the surface chemistry of carbon blacks and other carbons, *Carbon*, 32 (1994) 759–769.
- [26] M.V. de S. Pinto, D.L. da Silva and A.C.F. Saraiva, Obtenção e caracterização de carvão ativado de caroço de buriti (*Mauritia flexuosa* L. f.) para a avaliação do processo de adsorção de cobre (II), *Acta Amaz.*, 43 (2013) 73–80.
- [27] A. Abbas, M.A. Hussain, M. Sher, M.I. Irfan, M.N. Tahir, W. Tremel, S.Z. Hussain, I. Hussain, Design, characterization and evaluation of hydroxyethylcellulose based novel regenerable supersorbent for heavy metal ions uptake and competitive adsorption, *Int. J. Biol. Macromol.*, 102 (2017) 170–180.
- [28] T.D. Šoštarić, M.S. Petrović, F.T. Pastor, D.R. Lončarević, J.T. Petrovića, J.V. Milojkovića, M.D. Stojanovića, Study of heavy metals biosorption on native and alkali-treated apricot shells and its application in wastewater treatment, *J. Mol. Liq.*, 259 (2018) 340–349.
- [29] S. Brunauer, P.H. Emmett, E. Teller, Adsorption of gases in multimolecular layers, *J. Am. Chem. Soc.*, 60 (1938) 309–319.
- [30] E.P. Barrett, L.G. Joyner, P.P. Halenda, The determination of pore volume and area distributions in porous substances, *J. Am. Chem. Soc.*, 73 (1951) 373–380.
- [31] A.C.A. Lima, R.F. Nascimento, F.F. Sousa, J.M. Filho, A.C. Oliveira, Modified coconut shell fibers: a green and economical sorbent for the removal of anions from aqueous solutions, *Chem. Eng. J.*, 185 (2012) 274–284.
- [32] D.M. Ruthven, Principles of Adsorption and Adsorption Process, John Wiley & Sons, New York, NY, 1984.
- [33] A.D. Luz, S.M.d.A.G.U. de Souza, C. da Luz, R.V.D.P. Rezende, A.A.U. de Souza, Multicomponent adsorption and desorption of BTX compounds using coconut shell activated carbon: experiments, mathematical modeling, and numerical simulation, *Ind. Eng. Chem. Res.*, 52 (2013) 7896–7911.
- [34] A. Shahbazi, H. Younesi, A. Badiei, Functionalized SBA-15 mesoporous silica by melamine-based dendrimer amines for adsorptive characteristics of Pb(II), Cu(II) and Cd(II) heavy metal ions in batch and fixed bed column, *Chem. Eng. J.*, 168 (2011) 505–518.
- [35] B.E. Grimwood, F. Ashman, Coconut Palm Products; Their Processing in Developing Countries, Food & Agriculture Organization, Rome, 1975.
- [36] F. Villacañas, M.F.R. Pereira, J.J.M. Órfão, J.L. Figueiredo, Adsorption of simple aromatic compounds on activated carbons, *J. Colloid Interface Sci.*, 293 (2006) 128–136.
- [37] Y. Zhu, P. Kolar, Investigation of adsorption of p-cresol on coconut shell-derived activated carbon, *J. Taiwan Inst. Chem. Eng.*, 68 (2016) 138–146.
- [38] S.J. Allen, G. Mckay, Adsorption isotherm models for basic dye adsorption by peat in single and binary component systems, *J. Colloid Interface Sci.*, 280 (2014) 322–333.
- [39] C.B. Vidal, D.Q. Melo, G.S.C. Raulino, A.D. Luz, C. Luz, R.F. Nascimento, Multielement adsorption of metal ions using Tururi fibers (*Manicaria Saccifera*): experiments, mathematical modeling and numerical simulation, *Desal. Water Treat.*, 57 (2015) 9001–9008.
- [40] M.S. Sreekala, M.G. Kumaran, S. Thomas, Oil palm fibers: morphology, chemical composition, surface modification, and mechanical properties, *J. Appl. Polym. Sci.*, 66 (1997) 821–835.
- [41] X. He, X. Liu, B. Nie, D. Song, FTIR and Raman spectroscopy characterization of functional groups in various rank coals, *Fuel*, 206 (2017) 555–563.
- [42] Z. Sun, L. Chai, Y. Shu, Q. Li, M. Liu, D. Qiu, Chemical bond between chloride ions and surface carboxyl groups on activated carbon, *Colloids Surf., A*, 530 (2017) 53–59.
- [43] R.M. Silverstein, F.X. Webster, D.J. Kiemle, D.L. Bryce, Identificação Espectrométrica de Compostos Orgânicos, 8 ed., LTC, New York, NY, 2006.
- [44] M. Baysal, A. Yürüm, B. Yıldız, Y. Yürüm, Structure of some western Anatolia coals investigated by FTIR, Raman, 13C solid

- state NMR spectroscopy and X-ray diffraction, *Int. J. Coal Geol.*, 163 (2016) 166–176.
- [45] H. Song, G. Liu, J. Zhang, J. Wu, Pyrolysis characteristics and kinetics of low rank coals by TG-FTIR method, *Fuel Process. Technol.*, 156 (2017) 454–460.
- [46] F. Wang, Y. Pan, P. Cai, T. Guo, H. Xiao, Single and binary adsorption of heavy metal ions from aqueous solutions using sugarcane cellulose-based adsorbent, *Bioresour. Technol.*, 241 (2017) 482–490.
- [47] S. Mohan, R. Gandhimathi, Removal of heavy metal ions from municipal solid waste leachate using coal fly ash as an adsorbent, *J. Hazard. Mater.*, 169 (2009) 351–359.
- [48] V. Kumar, Y.K. Bhardwaj, K.P. Rawat, S. Sabharwal, Radiation-induced grafting of vinylbenzyltrimethylammonium chloride (VBT) onto cotton fabric and study of its anti-bacterial activities, *Radiat. Phys. Chem.*, 73 (2005) 175–182.
- [49] C. Appel, L.Q. Ma, R.D. Rhue, E. Kenneley, Point of zero charge determination in soils and minerals via traditional methods and detection of electroacoustic mobility, *Geoderma*, 113 (2003) 77–93.
- [50] N. Singh, C. Balomajumder, Simultaneous removal of phenol and cyanide from aqueous solution by co-culture of strain immobilized onto coconut shell activated carbon, *Desal. Water Treat.*, 57 (2016) 26136–26152.
- [51] A.A.d.A. Alves, G.L.d.O. Ruiz, T.C.M. Nonato, L.C. Müller, M.L. Sens, Performance of the fixed-bed of granular activated carbon for the removal of pesticides from water supply, *Environ. Technol.*, 40 (2019) 1977–1987.
- [52] T.G. Kebede, A.A. Mengistie, S. Dube, T.T.I. Nkambule, M.M. Nindi, Study on adsorption of some common metal ions present in industrial effluents by *Moringa stenopetala* seed powder, *J. Environ. Chem. Eng.*, 6 (2018) 1378–1389.
- [53] L. Liu, S. Liu, H. Peng, Z. Yang, L. Zhao, A. Tang, Surface charge of mesoporous calcium silicate and its adsorption characteristics for heavy metal ion, *Solid State Sci.*, 99 (2020) 106072.
- [54] D. Huang, B. Xu, J. Wu, P.C. Brookes, J. Xu, Adsorption and desorption of phenanthrene by magnetic graphene nano-materials from water: roles of pH, heavy metal ions and natural organic matter, *Chem. Eng. J.*, 3768 (2019) 390–399.
- [55] D.Q. de Melo, C.B. Vidal, T.C. Medeiros, G.S. Raulino, A. Dervanoski, M.C. Pinheiro, R.F. Nascimanto, Biosorption of metal ions using a low cost modified adsorbent (*Mauritia flexuosa*): experimental design and mathematical modeling, *Environ. Technol.*, 37 (2016) 2157–2171.
- [56] A.K. Meena, K. Kadirvelu, G.K. Mishra, C. Rajagopal, P.N. Nagar, Adsorption of Pb(II) and Cd(II) metal ions from aqueous solutions by mustard husk, *J. Hazard. Mater.*, 150 (2008) 619–625.
- [57] S. Guiza, Biosorption of heavy metal from aqueous solution using cellulosic waste orange peel, *Ecol. Eng.*, 99 (2017) 134–140.
- [58] N. Feng, X. Guo, S. Liang, Y. Zhu, J. Liu, Biosorption of heavy metals from aqueous solutions by chemically modified orange peel, *J. Hazard. Mater.*, 185 (2011) 49–54.
- [59] P.S. Kumar, S. Ramalingam, S.D. Kirupha, A. Murugesan, T. Vidhyadevi, S. Sivanesan, Adsorption behavior of nickel(II) onto cashew nut shell: equilibrium, thermodynamics, kinetics, mechanism and process design, *Chem. Eng. J.*, 167 (2011) 122–131.
- [60] P.S. Kumar, S. Ramalingam, V. Sathyaselvabala, S.D. Kirupha, S. Sivanesan, Removal of copper(II) ions from aqueous solution by adsorption using cashew nut shell, *Desalination*, 266 (2011) 63–71.
- [61] B. Singha, S.K. Das, Biosorption of Cr(VI) ions from aqueous solutions: kinetics, equilibrium, thermodynamics and desorption studies, *Colloids Surf., B*, 84 (2011) 221–232.
- [62] B. Singha, S.K. Das, Adsorptive removal of Cu(II) from aqueous solution and industrial effluent using natural/agricultural wastes, *Colloids Surf., B*, 107 (2013) 97–106.
- [63] R. Leyva-Ramos, L.A. Bernal-Jacome, I. Acosta-Rodriguez, Adsorption of cadmium(II) from aqueous solution on natural and oxidized corncob, *Sep. Purif. Technol.*, 45 (2005) 41–49.
- [64] M. Thirumavalavan, Y.L. Lai, L.C. Lin, J.F. Lee, Cellulose-based native and surface modified fruit peels for the adsorption of heavy metal ions from aqueous solution: Langmuir adsorption isotherms, *J. Chem. Eng. Data*, 55 (2010) 1186–1192.
- [65] I. Langmuir, The adsorption of gases on glass, mica and platinum, *J. Am. Chem. Soc.*, 345 (1914) 1361–1368.
- [66] H. Freundlich, Über die Adsorption in Lösungen, *Z. Phys. Chem.*, 57 (1906) 385–470.